Reaction Dynamics of C(^{3}P) with Chloroform

J.-H. Choi,† M. R. Scholefield, D. Kolosov, and H. Reisler*

Department of Chemistry, University of Southern California, Los Angeles, California 90089-0482

Received: March 19, 1997; In Final Form: June 16, 1997[⊗]

The reaction of carbon(^{3}P) with chloroform ($CHCl_3$) was studied in a crossed-beam configuration. C(^{3}P) was produced by laser ablation of graphite, and its translational energy was varied by seeding in carrier gases to investigate the reaction mechanism in two center-of-mass energy regimes: a low-energy regime of 3.2 and 5.3 kcal/mol and a high-energy regime peaked at 85 kcal/mol. The CCl reaction product was probed by laser-induced fluorescence via the $A^2\Delta \leftarrow X^2\Pi$ ($\Delta v = 0$) transition. In the low-energy regime, CCl was observed to be highly rotationally excited ($T_{rot} = 1500-1800$ K), and the first excited vibrational level was significantly populated. Good agreement was obtained between the experimental results and statistical estimations based on prior calculations, suggesting that the reaction proceeds through an insertion complex and that the exit channel does not exhibit distinct dynamical biases. In the high-energy regime, however, the reaction pathway is believed to involve a short-lived complex that preferably samples reactants from the broad center-of-mass energy distribution with *lower collision energy components*. Contributions from an abstraction mechanism cannot be ruled out.

I. Introduction

Atomic carbon is one of the smallest elements that participates in abstraction, addition, and insertion reactions, important in combustion, interstellar space, and synthetic hydrocarbon chemistry.[1,2] In addition, with only six electrons and a small energy gap (1.26 eV) between the ground state (^{3}P) and the first excited state (^{1}D), atomic carbon is amenable to both theoretical and experimental investigations of the effects of its electronic configuration on reaction pathways. Despite its mechanistic importance, difficulties in generating carbon atoms state selectively and reliably have resulted in fewer studies of its reactions compared with hydrogen and other second-row atomic species. Generation of atomic carbon by photolysis of carbon suboxide produces a mixture of its spin states, as well as the reactive species C_2O.[3] In contrast, laser ablation of graphite can be used to generate an efficient, clean, and state-selective beam of C(^{3}P).[4−8] This technique, combined with pulsed, crossed molecular beams, is useful for detailed studies of carbon atom reactions under single-collision conditions with well-defined energies.[5,7,8]

In previous studies that investigated the endothermic reactions of hyperthermal C(^{3}P) with several molecules including H_2, HCl, HBr, and CH_3OH, experimental and theoretical work suggested that an insertion pathway involving the participation of carbene intermediates may be the primary reaction mechanism.[6,9] This was also borne out in trajectory calculations on the C(^{3}P) + H_2 and HCl reactions, where the observed internal distributions were successfully reproduced.[10] The feasibility of an insertion mechanism for reactions of C(^{3}P), as opposed to those of O(^{3}P) for which barriers to insertion are dictated by orbital repulsion in the entrance valley,[11] opens the possibility of using these reactions to activate saturated hydrocarbons, a usually difficult task. Insertion has also been implicated in earlier studies of such reactions by Skell and co-workers, in which carbon species generated by a carbon arc and reacting in the condensed phase (∼77 K) give rise to products in which atomic carbon is incorporated into the reactant hydrocarbon.[12] Since little is known about the detailed mechanisms of these reactions, our goal here is to study an *exothermic* reaction of C(^{3}P) with a saturated hydrocarbon in order to elucidate the role of insertion. The high-energy carbon source used in our previous study of endoergic reactions has a broad range of energies; thus, effects due to collision energy cannot be studied, and mechanisms are sometimes obscured.

In this paper, we describe our investigation of translational energy effects on the reaction of C(^{3}P) with chloroform,[13]

$$C(^3P) + CHCl_3 \rightarrow CCl + CHCl_2 \qquad \Delta H = -19.4 \pm 5.4 \text{ kcal/mol} \quad \text{(Ia)}$$

$$\rightarrow CH + CCl_3 \qquad \Delta H = +14.4 \pm 3.4 \text{ kcal/mol} \quad \text{(Ib)}$$

$$\rightarrow HCl + C_2Cl_2 \qquad \Delta H = -118.7 \pm 5.5 \text{ kcal/mol} \quad \text{(Ic)}$$

$$\rightarrow CHCl + CCl_2 \qquad \Delta H = -24.6 \pm 7.2 \text{ kcal/mol} \quad \text{(Id)}$$

at two distinct collision energy regimes. Using two separate techniques known as free laser ablation and seeded laser ablation to generate well-defined atomic carbon beams, collision energies of ∼85, 5.3, and 3.2 kcal/mol are obtained for the C + $CHCl_3$ system. At the highest collision energies, both diatomic products CCl and CH are observed using laser-induced fluorescence detection; however, for the reaction channel leading to CH, no quantitative data could be obtained due to small signal levels. For all collision energies, spectral simulations are used to assign CCl rotational temperatures and the vibrational energy partitioning into the low level states, and the results are compared with statistical prior distributions to elucidate the reaction mechanism of reaction Ia.

II. Experimental Section

The crossed-beam apparatus consists of an ablation chamber, a molecular beam chamber, and an octagonal reaction chamber, each pumped separately by a diffusion pump. For the data

† Present address: Department of Chemistry, Korea University, 1 Anam-Dong Sunbuk-Ku, Seoul, Korea 136-701.

[⊗] Abstract published in *Advance ACS Abstracts,* August 1, 1997.

S1089-5639(97)00999-7 CCC: $14.00

presented here, only the ablation chamber is differentially pumped (through a 3 mm skimmer). Average background pressures with both beams on are $\sim 3 \times 10^{-5}$ Torr, while operating at 10 Hz.

The ground-state atomic carbon beam, C(^{3}P), is generated by laser ablation of graphite.[4−8] The fourth harmonic output (266 nm) of a Nd:YAG laser (Spectra-Physics GCR-11-3, 7 ns) is focused to an approximately 0.5 mm diameter spot (50 cm focal-length lens) at the surface of a spectroscopic grade graphite rod (Bay Carbon Inc.) maintained in constant helical motion for good shot-to-shot stability.

The apparatus is designed to generate atomic carbon in two different modes. In the first mode, ablated carbon atoms are allowed to expand freely into the chamber vacuum (*free* ablation). The ablation laser beam passes directly through the carbon beam skimmer to hit the graphite rod, generating a counterpropagating, translationally "hot" (∼3 eV), pulsed atomic beam of short temporal duration (6 μs fwhm at a distance of 60 mm from the rod).[6] Although the spread in carbon atom velocities is large, free ablation is advantageous in that almost complete destruction of C_n cluster species is achieved at the moderate ablation energies used (3−4 mJ). In the second mode, the ablated atoms are entrained in a carrier gas to allow kinetic energy control of the reactant atom beam (*seeded* ablation). In this configuration, the rod holder is coupled to the faceplate of a magnetic induction-type pulsed supersonic valve (R. M. Jordan Co., 0.5 mm diameter orifice, 50 μs pulse fwhm), with the graphite rod recessed by ∼4 mm to the valve nozzle. This type of pulsed valve has been chosen due to its ability to produce gas pulses of short temporal duration and high peak intensities, both of which are paramount to generating an efficient seeded beam. The ablation laser is fired as the seeding gas pulse emitted by the pulsed valve passes through the ablation region (typically 50−60 μs after triggering the Jordan valve), thus entraining the ablated carbon species prior to expanding into the chamber through the skimmer. Here, the ablation laser enters the chamber in a direction orthogonal to the propagation of the seeded beam. In this experiment, He and a 30% Ne:70% He mixture are used as carrier gases at stagnation pressures of 100 psi (∼7.5 atm). Higher energies, e.g., 5−6 mJ, are required for seeded ablation, in order to compensate for the lower carbon atom densities due to losses from increased C_n clustering in the entrained beam. The carbon rod is placed at distances of 60 and 70 mm from the reaction center for free and seeded ablation, respectively, and ∼15 mm from the carbon beam skimmer. No metastable states of atomic carbon (^{1}D,^{1}S) have been observed in either free or seeded laser ablation of graphite.[4,6,7]

Although the distribution of C_n species has not been directly measured by this group, the amount of C_3 (the most stable of the small C_n species) in the seeded atomic beam is considered to be small. C_3(A←X) background fluorescence can be observed simultaneously with CN(B←X) fluorescence (a primary product of the reaction of C(^{3}P) + N_2O) in our seeded ablation system. With careful adjustment of the ablation focusing lens, C_3 signals can be effectively minimized and CN signals (hence C(^{3}P)) maximized,[7] and typical signal ratios of C_3 to CN are less than 1 to 6. In addition to this, Kaiser *et al.*[8] have also generated an atomic beam of carbon using a similar seeded ablation design. With TOF-MS, they have determined the ratio of C_1:C_2:C_3 ablated species in helium gas to be 1:0.06:0.07.

A supersonic molecular beam of chloroform is generated by bubbling He through $CHCl_3$ (Fisher Scientific Co.) in an ice/water bath to obtain a ∼5% $CHCl_3$/He mixture and then expanding through a pulsed supersonic valve (General Valve, 0.8 mm diameter orifice, 650 μs pulse fwhm). Typical stagnation pressures are 550−800 Torr at ∼300 K. The pulsed valve is heated to ca. 80 °C to minimize formation of clusters and is typically placed at 40 mm from the reaction center. The neutral beam is unskimmed to obtain a higher signal-to-noise (S/N) ratio.

The CCl reaction product is detected by laser-induced fluorescence (LIF) via the $A^2\Delta \leftarrow X^2\Pi$ ($\Delta v = 0$) transition at ∼278 nm,[14−16] using the frequency-doubled output (KDP, Inrad AT-II autotracker) of an excimer-pumped dye laser system (Questek 2220M and Lambda Physik FL2001) operating on Coumarin 540A dye. The probe beam is loosely focused to a ∼3 mm diameter spot at the reaction center by a 1 m focal-length lens. The resulting fluorescence is imaged using a Galileo type telescope through a 279.0 ± 5.5 nm interference filter (Corion) onto the PMT (GaAs Hamamatsu R943-02). For free ablation, the probe laser pulse is delayed by ∼6 μs with respect to the firing of the ablation laser, for seeded ablation in He by ∼42 μs, and for seeded ablation in 30% Ne:70% He by ∼68 μs.

Analog signals from the PMT are sent to a Nicolet Explorer II digital oscilloscope interfaced to an IBM-compatible PC for data storage and processing. The timing sequence of the experiments is controlled by an array of pulse and delay generators allowing control of six separate channels with 10 ns incremental time resolution.

III. Results and Analysis

1. Center-of-Mass Collision Energies. Velocity distributions of the atomic carbon beam generated by free ablation have been characterized in detail by determining its time-of-flight (TOF) distribution.[6] The directional, monomeric beam possesses a peak velocity of ∼8000 m s^{-1} with a broad velocity distribution of about 6000 m s^{-1} fwhm.

In this work, velocity distributions for the seeded atomic beams are estimated from C_3 TOF data, since the latter is always present in the seeded beams and is easy to detect by LIF via the Swing bands ($A^1\Pi_u \leftarrow X^1\Sigma_g^+$).[18] Assuming that all small ablated C_n species are fully entrained in the carrier gas, C_3 and atomic carbon will have similar velocities in the seeded beam. TOF data are collected by monitoring the C_3 LIF signal at 387.2 nm as a function of the ablation−probe delay, at a fixed distance of 70 mm between the graphite rod and the excitation laser. The TOF distributions obtained are then converted to velocity distributions as described elsewhere.[6] Carbon atoms seeded in He have a peak velocity at 1630 m s^{-1} with a narrow velocity distribution of 250 m s^{-1} fwhm, while those seeded in 30% Ne:70% He have a peak velocity of 1035 m s^{-1} with a velocity distribution of 220 m s^{-1}. The velocity of the 5% $CHCl_3$/He gas mixture is estimated at 1180 m s^{-1} using calculations that assume a full expansion of the molecular beam.[19]

Center-of-mass (com) collision energies are subsequently obtained using the experimentally determined carbon velocities and the calculated velocity for the molecular beam. The com collision energies for the C + $CHCl_3$ system are 85 ± 50 (fwhm) kcal/mol for free ablation, 5.3 ± 0.6 kcal/mol for seeding in He, and 3.2 ± 0.5 kcal/mol for seeding in a 30% Ne:70% He mixture (Table 1).

2. CCl($X^2\Pi$) Internal State Distributions and Spectral Simulations. The CCl($^2\Pi$) product is detected by LIF via the $A^2\Delta \leftarrow X^2\Pi$ ($\Delta v = 0$) transition. Spectra obtained for all three collision energy regimes are displayed in Figure 1. Large CCl signals are observed for both free ablation and seeded ablation in pure He; however, this signal is reduced by over half on

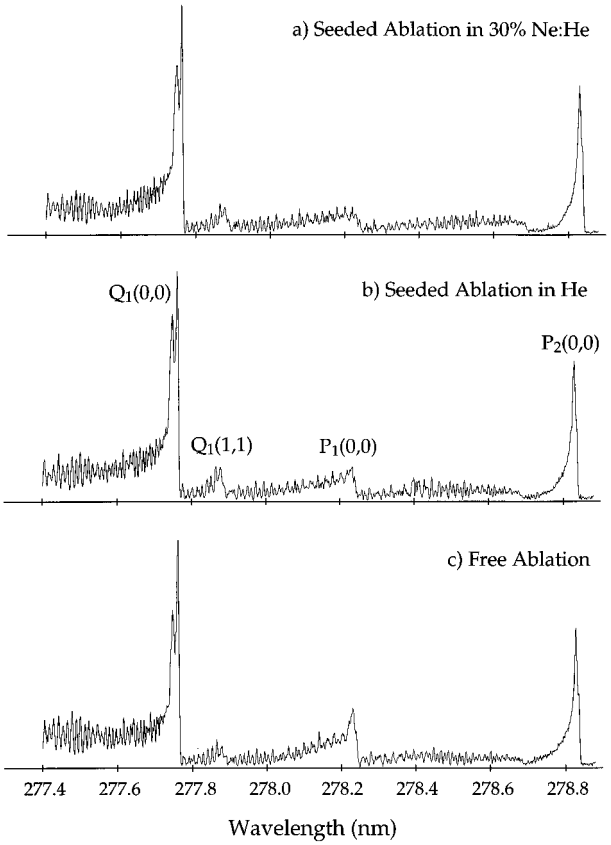

Figure 1. Experimental CCl($A^2\Delta \leftarrow X^2\Pi$) $\Delta v = 0$ LIF spectra obtained in the reaction of $C(^3P)$ and $CHCl_3$. The $C(^3P)$ is generated by (a) seeded ablation in 30% Ne:70% He, (b) seeded ablation in pure He, and (c) free ablation.

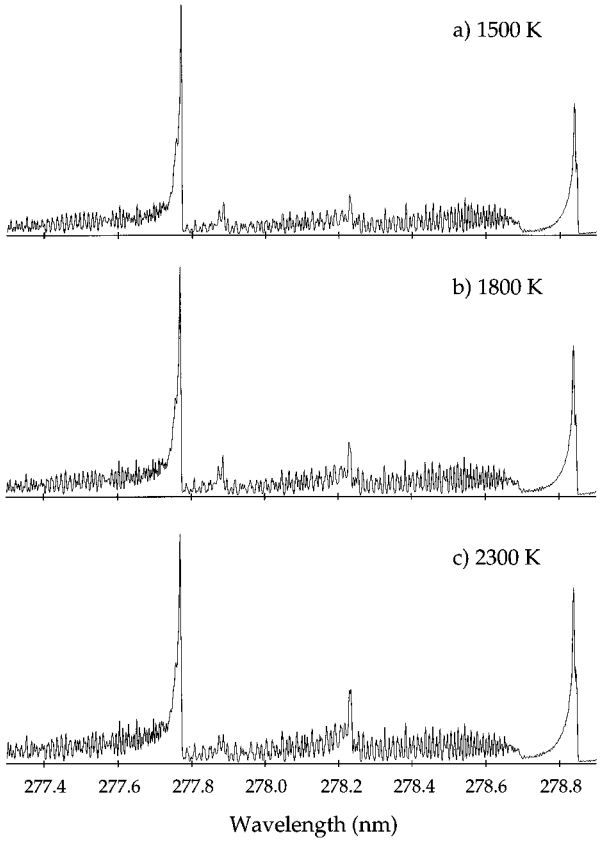

Figure 2. Simulated CCl($A^2\Delta \leftarrow X^2\Pi$) $\Delta v = 0$ LIF spectra, obtained using the formulas given in refs 15 and 20, and spectroscopic constants given in ref 15. The simulations correspond to CCl rotational temperatures of (a) 1500 K, (b) 1800 K, and (c) 2300 K.

switching to the Ne:He mix, due to the greater degree of clustering in the heavier carrier gas mixture. The (0,0) band of the $A \leftarrow X$ transition is the strongest for CCl; however, the near equality of the molecular constants of the X and A states results in crowded vibrational bands, and at high rotational temperatures the spectrum is congested due to rotational band overlap. Fortunately, several branches form prominent bandheads,[14−16] and the Q_1, P_1, and P_2 bandheads of the (0,0) band and the Q_1 bandhead of the (1,1) band are all clearly observed in the spectra. Although CH was observed in the reaction of $C(^3P)$ generated by free ablation with $CHCl_3$ (reaction Ib), signal levels were too poor to obtain internal state information.

From the experimental spectra, it is clear that the CCl product exhibits considerable rotational excitation in both collision energy regimes. The $P_1(0,0)$ bandhead in particular is a sensitive measure of rotational excitation, as it forms at $60 < j'' < 70$ (corresponding to $E_{rot} > 2400$ cm^{-1}),[16] and is observed in all cases, although a marked decrease in the bandhead height is observed as the collision energy of the $C + CHCl_3$ system is decreased. As this bandhead will also rapidly disappear under conditions of rotational relaxation, it was used to ensure that the spectra are obtained under single-collision conditions. A series of scans taken at various nozzle−interaction region distances (30−60 mm) and stagnation pressures (550−800 Torr) produced no significant change in the relative size of the P_1 bandhead, verifying that relaxation is minimal. The CCl product also displays some vibrational excitation, as is evidenced by the appearance of the $Q_1(1,1)$ bandhead in all experimental spectra.

To obtain estimates of the rotational temperatures and the vibrational partitioning between the ground and first excited states in the nascent CCl($X^2\Pi$) state, the experimental spectra are compared to simulations of the $A \leftarrow X$ transition generated using known spectroscopic constants.[15] The rotational line strengths of the $A \leftarrow X$ system are calculated using the formulas given by Kovacs.[20] Although spectroscopic Franck−Condon factors for the diagonal bands have not been experimentally determined, they are expected to be large due to similar molecular constants in the X and A states, and calculations have yielded values of 0.988 and 0.963 for the (0,0) and (1,1) bands, respectively.[21] The best fits of the simulations to the experimental data are obtained by using the relative vibrational populations, spectral bandwidth, and rotational temperatures for the $v'' = 0$ and $v'' = 1$ levels as fitting parameters, and the simulated spectra thus obtained are displayed in Figure 2. Due to the poor sensitivity of the simulations to the rotational temperature of $v'' = 1$, similar temperatures were used for both bands, while the rotational excitation in each vibrational band was truncated at the highest level allowed by energetics.

The spectral simulations most closely match the experimental spectra at CCl rotational temperatures of 2300 ± 500 K for free ablation, 1800 ± 300 K for seeded ablation in He, and 1500 ± 300 K for seeded ablation in 30% Ne:70% He. In the simulations, Boltzmann distributions are assumed for each vibrational level. The best agreement with the experimental spectra is obtained when the vibrational level partitioning into $v'' = 1$ compared to $v'' = 0$ is 20% for free ablation, 35% for seeded ablation in He, and 30% for seeded ablation in the Ne:He mix. However, these ratios do not reflect the true vibrational partitioning, since the analysis should also take into account the Franck−Condon corrections (0.988 and 0.963 for the (0,0) and (1,1) bands, respectively) and the lifetime (τ) differences of the $v' = 0$ and $v' = 1$ states. Predissociation in the $A^2\Delta$ state of CCl reduces the collision-free lifetime of 110 ns in v'

$= 0$ (independent of rotational quantum number) to 35 ns for the F_1 spin−orbit component of $v' = 1$.[17] The corrections were performed using the following formula,

$$\frac{n(v''=1)}{n(v''=0)} = \frac{I(Q_1(1,1))}{I(Q_1(0,0))}\frac{\tau_0}{\tau_1}\frac{\mathrm{FC}(0,0)}{\mathrm{FC}(1,1)} \quad (1)$$

where I and FC are the intensity and the Franck−Condon factor of each Q_1 branch in the spectrum, and τ_v is the lifetime of each excited vibrational level. It is thus estimated that the vibrational level partitioning is 36 ± 9% for free ablation, 53 ± 8% for seeded ablation in He, and 42 ± 8% for seeded ablation in 30% Ne:70% He. As the (2,2) band cannot be observed in the $\Delta v = 0$ sequence due to strong overlap by other bands, the $\Delta v < 0$ sequences were investigated in an attempt to detect population in the higher vibrational levels. No noticeable band features were observed due to a low S/N ratio, as might be expected from poor Franck−Condon factors and high predissociation rates. Thus, population in higher vibrational levels could not be ascertained.

IV. Discussion

Nascent internal distributions of the CCl($X^2\Pi$) product obtained under single-collision conditions can provide insights into the reactive processes, including energy disposal into products and its dependence on experimental conditions.[22] The total available energy E_{avl} for partitioning between internal degrees of freedom and recoil velocity of the reaction products in reaction Ia is given by the following expression:

$$E_{avl} = E_{com} + E_{int}(CHCl_3) - \Delta H_{rxn} \quad (2)$$

E_{com} is the center-of-mass collision energy of the reactive system as described in section III.1, $E_{int}(CHCl_3)$ is the internal energy of chloroform and is assumed to be negligible in the supersonic molecular beam, and ΔH_{rxn} is the reaction enthalpy and is calculated to be −19.4 kcal/mol for the exothermic reaction Ia. The available energy for the $C + CHCl_3$ system is thus estimated to be 104 ± 55 kcal/mol for free ablation (recall the very broad distribution of E_{com}), 24.7 ± 6 kcal/mol for seeding in He, and 22.6 ± 6 kcal/mol for seeding in a 30% Ne:70% He mixture. As it is useful to discuss energy disposal and reaction mechanisms in terms of low (seeded ablation) and high (free ablation) collision energy regimes, the remaining discussion is divided into these sections.

1. Reaction in the Low Collision Energy Regime. As discussed in the previous section, the observed nascent CCl rotational excitation shows good agreement with simulated spectra based upon a Boltzmann-like distribution and does not exhibit clear dynamical biases. Thus, it is useful to compare the observed distributions to those predicted by statistical models. For polyatomic systems, the simplest approach is to compare with prior distributions, which are determined by the available volumes in phase space of the fragments, and are constrained only by energy conservation.[23] In the case of a reaction producing diatomic and polyatomic fragments (reaction Ia), the prior distribution for CCl in a specific rovibrational state, $P(j,v)$ is obtained using

$$P(j,v) \propto (2j+1)n(E_v)\sum_V \rho(E_V)(E_{avl} - E_j - E_v - E_V)^2 \quad (3)$$

where $(2j + 1)$ is the rotational degeneracy of the diatomic CCl and $n(E_v)$ is the degeneracy of CCl vibrational states, which is unity for a diatomic molecule. The summation is obtained through integrations over the 3-D translational density of states using the reduced mass (μ) of CCl and $CHCl_2$ and the classical rotational density of states of the $CHCl_2$ product. The vibrational density of states is obtained using direct count of states. The only quantities necessary to determine $P(j,v)$ are the $CHCl_2$ vibrational frequencies for calculating $\rho(E_V)$, and these are obtained from the *ab initio* calculations of Hopkinson and coworkers.[24] From the predicted CCl internal state distributions, both rotational temperatures and the ratios of the two vibrational state populations are obtained. The results are summarized in Table 1. The calculated rotational distributions appear Boltzmann-like over a broad range, and are therefore assigned "temperatures" based on >90% of the populated levels. Only states in the interval between the low and high rotational levels shown in Figure 3 are used to obtain the rotational temperatures shown in Figure 4. In this manner, effects due to possible relaxation of low j's, and the thermal distribution of reagent energies which affects the high j limit are avoided. The vibrational state distributions are obtained by summing over the entire rotational prior distribution for each vibrational level to obtain its relative population. The experimental rotational temperatures and the ratio $P(v''=1):P(v''=0)$ obtained with C(^{3}P) seeded in He and the 30% Ne:70% He mixture are consistent with the prior calculations that apportion the population of each state as per its degeneracy. Although detailed balance is not obeyed in the prior calculations and angular

TABLE 1: Summary of Experimental and Prior Results for CCl Rotational Temperatures and Relative Vibrational Partitioning, Obtained at the Collision Energies Achieved by Free and Seeded Ablation Techniques

	collision energy (kcal/mol)	simulated spectra		prior calculations	
		T_{rot} (K)[a]	v_1/v_0	T_{rot} (K)[a]	v_1/v_0
free ablation	85 ± 50 (fwhm)	2300 ± 400	0.36 ± 0.09	6004	0.82
He	5.3 ± 0.6	1800 ± 300	0.53 ± 0.08	1763	0.49
30% Ne:He	3.2 ± 0.5	1500 ± 300	0.42 ± 0.08	1618	0.46

[a] Rotational temperatures are reported for $v = 0$ only.

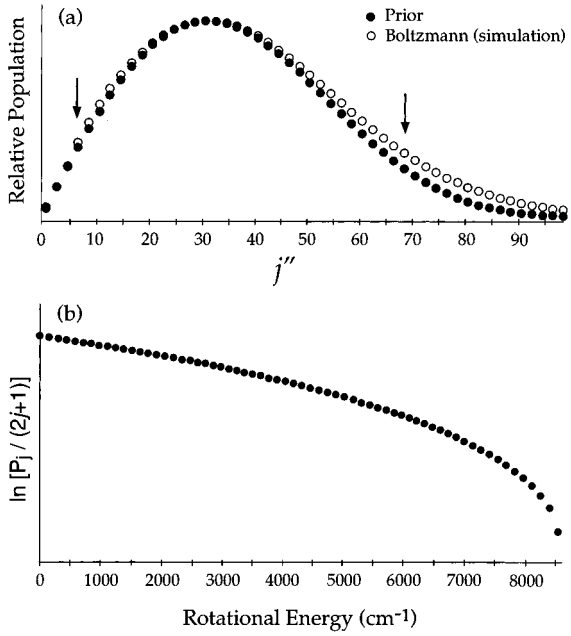

Figure 3. (a) CCl $v'' = 0$ prior distribution obtained using an average available energy of 24.7 kcal/mol, corresponding to a rotational temperature of 1763 K (●). Also displayed is the Boltzmann distribution used to generate the CCl simulated spectrum at 1800 K (○). (b) Boltzmann plot of the CCl prior distribution in (a). Arrows in (a) indicate the interval of j states that are used to assign rotational temperatures to CCl.

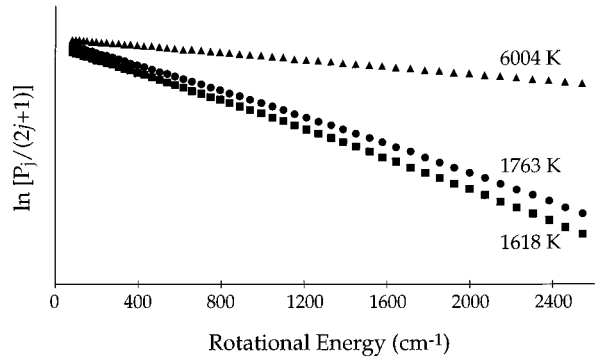

Figure 4. Boltzmann plots of the CCl $v'' = 0$ prior distributions obtained at available energies of 104 (▲), 24.7 (●), and 22.6 kcal/mol (■). The plots correspond to rotational temperatures of 6004, 1763, and 1618 K, respectively (see Figure 3 and the text).

momentum conservation is neglected, these do not significantly affect the calculated distributions.

The agreement between the prior distributions and the results of the seeded ablation experiments implies that in the low collision energy regime the reaction proceeds through an insertion complex, $ClCCHCl_2$, which survives sufficiently long to allow the available energy to be statistically partitioned among all the degrees of freedom of the fragments prior to dissociating into CCl and $CHCl_2$. The energetics of the formation of the $ClCCHCl_2$ intermediate are unknown; however, in analogy with other carbene intermediates, it is likely to be considerably more stable than the reactants. Analogous carbene intermediates such as HCH, HCCl, and $HCCH_3$ are stable with respect to their reactants by 60−90 kcal/mol, irrespective of their spin states.[9,25]

Although the potential energy surface (PES) for the reaction of $C(^3P)$ with $CHCl_3$ is unknown, it is quite useful to compare reaction Ia to detailed *ab initio* calculations performed by Harding, Guadagnini, and Schatz (HGS) for the $C + H_2 \rightarrow CH_2$ system.[9] They obtained a global ground-state potential energy surface for all orientations of atomic carbon approach and found that H atom abstraction via a collinear $C_{\infty v}$ path along the $^3\Pi$ surface experiences a long-range repulsion and has a late barrier of 1.3 eV. However, a predominant insertive C_{2v} (C_s) pathway was calculated to form the triplet methylene intermediate without any activation barrier, which may then dissociate to form the fragment products CH and H. These authors find an attractive long-range interaction for an approach in which the empty p orbital of carbon points toward H_2, leading to an excited methylene triplet state. However, when a singly occupied carbon p orbital points toward H_2, a large entrance barrier exists for formation of the ground state of the methylene intermediate. An avoided crossing between these states results in a reduction (or possible elimination) of the entrance channel barrier to insertion. More recent trajectory calculations by Guadagnini and Schatz on the endothermic $C(^3P) + HX$ (X = H, D, Cl) reactions have determined that, in the reaction with H_2, the carbon atom approach for reactive encounters is not perpendicular to the H_2 molecule (which is generally believed to be dominant for insertion), but rather is nearly collinear.[10] This nontraditional approach is attributed to inefficient energy transfer between the symmetric and asymmetric modes of the activated $^3CH_2$ intermediate in the perpendicular approach (less apparent in CHD and CHCl due to asymmetry). Comparisons of their predicted internal distributions to our experimental CH product distributions for the $C(^3P) + H_2$ reaction[6] show an excellent agreement, strongly supporting the accuracy of the HGS surface.

For the exothermic reaction Ia investigated here, the data suggest a similar insertion pathway. On the basis of the strong LIF signals obtained even at the lowest collision energies employed in our study ($E_{com} = 3.2$ kcal/mol), we conclude that only a small (if any) barrier exists in the entrance channel leading to the intermediate. We may speculate, however, that the insertion reaction is very likely affected by strong steric hindrances in the entrance channel, since the bulkier chloroform will restrict the angle of approach significantly and not all geometries will access the entrance valley; e.g., atomic carbon is more likely to approach between the H atom and a Cl atom. In addition, compared to the CH_2 intermediate described above, the symmetry of $ClCCHCl_2$ is obviously reduced, and the higher density of states of the polyatomic complex should increase the rate of energy flow among the internal degrees of freedom in the intermediate, facilitating a statistical outcome. The good agreement between the experimental and statistical distributions also indicates that, after passing through the transition-state region, exit channel dynamics (e.g., a barrier or strong angular anisotropy) do not significantly influence the rotational excitation of CCl.

To the best of our knowledge, there are no other gas-phase studies of exoergic reactions of $C(^3P)$ with saturated hydrocarbons to which our results can be compared. Nishiyama *et al.* studied the exoergic reaction of carbon with HI and observed rotationally relaxed CH in both $v'' = 0$ and 1 at 300 K.[26] The vibrational population of $v'' = 1$ was found to be ca. 45% of that of $v'' = 0$, larger than that predicted by prior calculations (ca. 15%) which often underestimate the degree of vibrational excitation in reactions of small molecules. Also, this high population is considered a characteristic feature of the product distributions for light atom-transfer reactions.[27] In their pioneering studies, Skell and co-workers studied the reactions of atomic carbon produced in a carbon arc with solid hydrocarbons at ~77 K. They found products that in the case of unsaturated hydrocarbons were attributed to insertion by both $C(^3P)$ and $C(^1D)$.[12a,b] In the case of halogenated hydrocarbons, insertion products were observed, but the spin states of the atomic carbon responsible for the reaction were not identified.[12c] Recently, Kaiser *et al.* have performed crossed-beam experiments of carbon with unsaturated hydrocarbons, and they favor an addition mechanism to double or triple bonds.[28]

2. Reaction at the High Collision Energy Regime. In the case of free ablation, the much higher collision energies allow the investigation of both the endoergic CH channel Ib and the exoergic CCl channel Ia. However, much larger LIF signals have been obtained from the CCl product than from CH. The large propensity for formation of CCl is easily understood based on energetics, the ratio of Cl to H atoms in chloroform, and steric effects.

Due to the very broad range of carbon atom translational energies obtained in free ablation, the prior distribution was determined at the peak of the collision energy (i.e., 85 kcal/mol). As expected, the large amount of available energy results in very broad rovibrational prior distributions compared to those obtained at the lower collision energies (Table 1). However, the experimentally observed CCl rovibrational excitation can be described by a much lower rotational temperature and a smaller fraction of vibrational energy partitioned into $v'' = 1$ compared to statistical predictions. There are several explanations for this result. The first is that due to the expected shorter lifetime of the intermediate complex at high collision energies, the large available energy will not be completely redistributed as assumed in the simple prior model. Thus, the product energy distribution will not display statistical behavior. Since CCl is the newly formed bond, the $CHCl_2$ counterfragment (the "old" bond) is expected to have even lower internal energy, and the balance of energy would then be deposited in relative translation.

We thus expect a broader Doppler line width for each rotational CCl line (e.g., ~0.8 cm^{-1} for low-j levels of CCl in $v'' = 0$, compared with the 0.4 cm^{-1} bandwidth of the laser).[29] However, careful inspection of the spectra obtained at low and high collision energies shows no significant broadening of these rotational lines, and thus we do not favor this interpretation.

Another plausible alternative is that although the collision energy distribution is broad, the most important contribution to the CCl signal results from the *lower* collision energy components. In exoergic reactions, the cross section often decreases significantly as the translational energy increases as a result of the shorter interaction time. Therefore, the observed rovibrational distribution in the free ablation scheme might be ascribed to preferred sampling of reactants in the low collision energy regime, which would lead to internal distributions comparable to those obtained in the seeded scheme. Indeed, in the HGS calculations for the C(^{3}P) + H_2 system, it was shown that the high-energy contribution to the reaction is minimal and that the overall product CH internal distribution observed in our previous experiments was perfectly reproduced by sampling a small fraction of reactants with collision energies just above reaction threshold.[10] In free ablation, we found that production of atomic carbon is so efficient that even when only a small fraction of the collision energy distribution contributes to the reactive flux, products can be observed. The conclusion that the low-energy portion of the collision energy distribution is responsible for most of the CCl signal is reinforced by the small signal from the endoergic CH channel in the chloroform reaction compared with that obtained, for example, in the reaction of C(^{3}P) with C_2H_2, which also has a competing exothermic channel (C_3H + H).[30]

Another possibility for the deviations from statistical predictions is the increase in the contribution of Cl abstraction with the increase in collision energy. Abstraction will explain the small branching ratio into the CH channel, since access to the H atom will have a large steric hindrance. However, the CCl product state distributions are not characteristic of abstraction reactions.

Although not investigated in this experiment, reactions Ic and Id are also energetically accessible. Reaction Ic leads to the formation of closed-shell C_2H_2 and HCl products and is thus expected to have a high barrier. Although a spin-forbidden channel, the heavy chlorine species significantly reduces the degree of spin selectivity due to strong spin−orbit interactions, facilitating intersystem crossing. Reaction Id can yield stable singlet and/or triplet carbene products but involves rearrangement and therefore may be less efficient.

Acknowledgment. The authors thank Mr. Paul Jordan of the R. M. Jordan Co. for his technical assistance with the pulsed supersonic valve used in the seeded ablation work. This study was supported by the director, Office of Energy Research, Office of Basic Sciences, Chemical Sciences Division of the U.S. Department of Energy, under Grant DEFG03-88ER13959.

References and Notes

(1) For reviews, see: (a) Mackay, C. in *Carbenes*; Moss, R. A., Jones, M., Eds.; Wiley and Sons: New York, 1975; Vol. II. (b) Shevlin, P. B. In *Reactive Intermediates*; Abramovich, R. A., Ed.; Plenum: New York, 1980; Vol. I.

(2) Gaydon, A. G. *The Spectroscopy of Flames*, 2nd ed.; Chapman and Hall: London, 1974.

(3) (a) Anderson, D. J.; Rosenfeld, R. N. *J. Chem. Phys.* **1990**, *94*, 7857. (b) Strauss, C. E. M.; Kable S. H.; Chawla, G. K.; Houston, P. L. *J. Chem. Phys.* **1990**, *94*, 1837.

(4) Reid, S. A.; Winterbottom, F.; Scott, D. C.; de Juan, J.; Reisler, H. *Chem. Phys. Lett.* **1992**, *189*, 430.

(5) Scott, D. C.; Winterbottom, F.; Scholefield, M. R.; Goyal, S.; Reisler, H. *Chem. Phys. Lett.* **1994**, *222*, 471.

(6) Scholefield, M. R.; Goyal, S.; Choi, J.-H.; Reisler, H. *J. Phys. Chem.* **1995**, *99*, 14605.

(7) Costes, M.; Naulin, C.; Dorthe, G.; Daleau, G.; Joussot-Dubien, J.; Lalaude, C.; Vinckert, M.; Destor, A.; Vaucamps, C.; Nouchi, G. *J. Phys. E* **1989**, *22*, 1017.

(8) Kaiser, R. I.; Suits, A. G *Rev. Sci. Instrum.* **1995**, *66*, 5405.

(9) (a) Harding, L. B. *J. Phys. Chem.* **1983**, *87*, 441. (b) Harding, L. B.; Guadagnini, R.; Schatz, G. C. *J. Phys. Chem.* **1993**, *97*, 5472.

(10) Guadagnini, R.; Schatz, G. C. *J. Phys. Chem.* **1996**, *100*, 18944.

(11) (a) Luntz, A. C. *J. Chem. Phys.* **1980**, *73*, 1143. (b) Andresen, P.; Luntz, A. C. *J. Chem. Phys.* **1980**, *72*, 5842. (c) Howard, R. E.; McLean, A. D.; Lester, W. A. *J. Chem. Phys.* **1979**, *71*, 2412.

(12) (a) Skell, P. S.; Havel, J. S.; McGlinchey M. J. *Acc. Chem. Res.* **1973**, *6*, 97. (b) Skell, P. S.; Engel, R. R. *J. Am. Chem. Soc.* **1965**, *87*, 4663; **1966**, *88*, 3749, 4883; **1967**, *89*, 2912. (c) Skell, P. S.; Harris, R. F. *J. Am. Chem. Soc.* **1965**, *87*, 5807; **1969**, *91*, 4440.

(13) The energetics of the reactions are calculated for ground-state reactants and products by using heats of formation taken from: (a) Chase, M. W., Jr.; Davies, C. A.; Downey, J. R., Jr.; Frurip, D. J.; McDonald, R. A.; Syverud, A. N. *JANAF Thermochemical Tables*, 3rd ed., Part I; *J. Phys. Chem. Ref. Data* **1985**, *14* (Suppl. 1). (b) Yang, X.; Felder, P.; Huber, J. R. *Chem. Phys.* **1994**, *189*, 127. (c) Rodriquez, C. F.; Hopkinson, A. C. *J. Phys. Chem.* **1993**, *97*, 849. (d) Holmes, J. L.; Lossing, F. P. *J. Am. Chem. Soc.* **1988**, *110*, 7343. (e) Lias, S. G.; Karpas, Z.; Liebman, J. F. *J. Am. Chem. Soc.* **1985**, *107*, 6089.

(14) (a) Verma, R. D.; Mulliken, R. S. *J. Mol. Spectrosc.* **1961**, *6*, 419. (b) Gordon, R. D.; King, G. W. *Can. J. Phys.* **1961**, *39*, 252. (c) Merer, A. J.; Travis, D. N.; Watson, J. K. G. *Can. J. Phys.* **1966**, *44*, 447.

(15) (a) Mélen, F.; Houbrechts, Y.; Dubois, I.; Bredohl, H. *J. Phys. B: At. Mol. Phys.* **1983**, *16*, 2523. (b) Sharpe, S. W.; Johnson, P. M. *J. Mol. Spectrosc.* **1986**, *116*, 247.

(16) Robie, D. C.; De Juan, J.; Reisler, H. *J. Mol. Spectrosc.* **1991**, *150*, 296.

(17) (a) Larsson, M.; Blomberg, M.; Siegbahn, P. *Mol. Phys.* **1982**, *46*, 365. (b) Gottscho, R.; Burton, R. H.; Davis, G. P. *J. Chem. Phys.* **1982**, *77*, 5298.

(18) Gausset, L.; Herzberg, G.; Lagerqvist, A.; Rosen, B. *Astrophys. J.* **1965**, *142*, 45.

(19) Kolodney, E.; Amirav, A. *Chem. Phys.* **1983**, *82*, 269.

(20) Kovacs, I. *Rotational Structure in the Spectra of Diatomic Molecules*; American Elsevier: New York, 1969.

(21) Kusakabe, M.; Ito, Y.; Tokue, I. *Chem. Phys.* **1993**, *170*, 243.

(22) Levine, R. D.; Bernstein, R. B. *Molecular Reaction Dynamics and Chemical Reactivity*; Oxford University Press: New York, 1987.

(23) Zamir, E.; Levine, R. D. *Chem. Phys.* **1980**, *52*, 253.

(24) (a) Hopkinson A. C. Private communication. (v_1 = 323.06, v_2 = 547.82, v_3 = 794.01, v_4 = 939.36, v_5 = 1315.98, and v_6 = 3290.65. These frequencies were obtained from an MP2/6311G(d,p) calculation and are in cm^{-1}. Frequencies v_4 and v_5 are out-of-plane, and the remainder are in the plane. (b) Rodriquez, C. F.; Bohme, D. K.; Hopkinson, A. C. *J. Phys. Chem.* **1996**, *100*, 2942.

(25) (a) Irikura, K. K.; Goddard, W. A., III; Beauchamp, J. L. *J. Am. Chem. Soc.* **1992**, *114*, 48. (b) Scuseria, G. E.; Durán, M.; Maclagan, G. A. R.; Schaefer, H. F. III. *J. Am. Chem. Soc.* **1986**, *108*, 3248. (c) Sakai, S.; Deisz, J.; Gordon, M. S. *J. Phys. Chem.* **1989**, *93*, 1888.

(26) Nishiyama, N.; Sekiya, H.; Nishimura, Y. *J. Chem. Phys.* **1986**, *84*, 5213.

(27) (a) Polanyi, J. C. *Acc. Chem. Res.* **1972**, *5*, 161. (b) Polanyi, J. C.; Schreiber, J. L. In *Physical Chemistry, an Advanced Treatise*; Jost, W., Ed.; Academic: New York, 1974; Vol. 6A, p 383. (c) Parr, C. A.; Polanyi, J. C.; Wong, W. H. *J. Chem. Phys.* **1973**, *58*, 5.

(28) (a) Kaiser, R. I.; Lee, Y. T.; Suits, A. G. *J. Chem. Phys.* **1995**, *103*, 10395. (b) Kaiser, R. I.; Lee, Y. T.; Suits, A. G. *J. Chem. Phys.* **1996**, *105*, 8721.

(29) The only well-resolved rotational lines in the congested CCl spectra are the low-j lines (5.5−15.5) of the R_1 branch. The energy available for translation is estimated by subtracting the internal energy of CCl(v=0,j=10.5) and the average internal energy of the $CHCl_2$ fragment (approximated to be the same as that for CCl) from the total available energy (104 kcal/mol). The amount of translational energy allotted to each fragment is inversely proportional to the mass of each fragment; thus, slightly less than two-thirds of this energy should go into CCl translation and is estimated to be 61 kcal/mol. The rotational line width is then determined using the expression fwhm $\approx 2\varpi_0(v_{CCl}/c)$, where ϖ_0 is the frequency of the transition, v_{CCl} is the velocity of the CCl fragment, which is estimated to be 3280 m/s, and c is the speed of light. At ϖ_0 = 36 009.32 cm^{-1} (corresponding to j = 10.5), the line width is thus calculated to be 0.787 cm^{-1}.

(30) Scholefield, M. R.; Choi, J.-H.; Reisler, H. Manuscript in preparation.